# Numerical Simulation of Combustion in Direct Injection Diesel Engines. Application to Additional Heating Systems.

**Cédric Garnier*, Jérôme Bellettre, Mohand Tazerout**
**Ecole des Mines de Nantes**
**Department of Energetics and Environmental Engineering**
**La Chantrerie, 4 rue Alfred Kastler BP 20722 44307 Nantes cedex 3**
**France**

**Gwénaël Guyonvarch**
**Valeo Climate Control Inc.**
**Innovation Department**
**8, rue Louis Lormand 78321 La Verrière**
**France**

## Abstract

This paper focuses on the simulated performance and pollutant emissions of a direct injection diesel engine. A zero-dimensional – two-zone combustion model is described and used to develop a new correlation to predict indicated performance. The combustion model and its hypothesis are presented first. Numerical results are then compared with experiments on a direct injection diesel engine for validation. The model shows that engine performance is well correlated with different running settings. A new correlation to predict the indicated efficiency is thus proposed and its interest is demonstrated. Finally, this study leads to enhance a simulation tool previously created.
*Keywords:* combustion modelling, simulation tool, cold start, car heating.

## Nomenclature

| | |
|---|---|
| *AHS* | Additional Heating System |
| *BTDC* | Before Top Dead Center |
| $c_p$ | Specific heat at constant pressure [J/kg/K] |
| $c_v$ | Specific heat at constant volume [J/kg/K] |
| $d_s$ | Engine bore [m] |
| $E_a$ | Activation energy [J/mol/K] |
| *EGR* | Exhaust Gas Recirculation |
| $h$ | Enthalpy per mass unit [J/kg] |
| $h_g$ | Heat transfer coefficient [W/m$^2$/K] |
| $k$ | Reaction rate constant [m$^3$/mol/s] |
| *LHV* | Low Heating Value [J/kg] |
| $m$ | Mass [kg] |
| $N$ | Engine rotation speed [rev/min] |
| $P$ | Pressure [bar] |
| Q | Heat [J] |
| $R$ | Gas constant [J/kg/K] |
| $S$ | Area [m²] |
| $T$ | Temperature [K] |
| $T_m$ | Torque [N.m] |
| $u$ | Internal energy per mass unit [J/kg] |
| $u_{pis}$ | Mean piston speed [m/s] |
| $V$ | Volume [m$^3$] |
| $W$ | Work [J] |
| $x_b$ | Burned mass fraction [-] |

**Greek Letters**

| | |
|---|---|
| $\Delta$ | Variation |
| $\eta_i$ | Indicated efficiency [-] |
| $\eta_v$ | Volumetric efficiency [-] |
| $\phi$ | Equivalence ratio [-] |
| $\tau_{ID}$ | Ignition delay [s] |
| $\tau_{comp}$ | Engine compression ratio [-] |
| $\sigma$ | Quantity of air at stoechiometry [kg/kg] |

* corresponding author : e-mail: cedric.garnier@emn.fr, phone number: (+33) 2.51.85.82.96, fax (+33) 2.51.85.82.99

## Introduction

The quality of combustion significantly improved over the last few years thanks to severe antipollution standards (EURO IV in Europe). Consumption benefits are thus results of reduced heat losses towards the coolant circuit and the cabin heating system [1]. During unfavourable atmospheric conditions, acceptable comfort for the user is therefore provided with an Additional Heating System (AHS). Various studies describe cold start thermal deficit and compare the effectiveness of several technologies used by equipment suppliers [1,2,3].

Technical and financial constraints for AHS development have forced the emergence of computer aided engineering. The only constraints remain computing time, flexibility in use and adaptation to different engines. Pirotais [4,5,6] developed a complete simulation tool based on a single zone combustion model linked with nodal method for predicting available heat flux. Its objectives were to simulate the effects of different AHS and analyse global car behaviour during cold starts. The interactions between the engine and cabin heating systems are solved by computing the instantaneous heat transfer from the combustion chamber. The global model architecture (Fig. 1) requires cartography of heat losses towards the coolant loop (Fig. 2), depending on engine load and speed conditions described by a driving cycle. An example of simulation results regarding a warm up test is presented in Fig. 3.

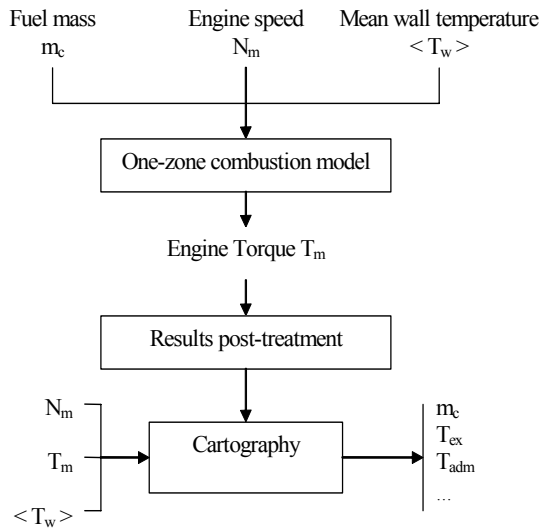


Figure 1 - Global model architecture [6].

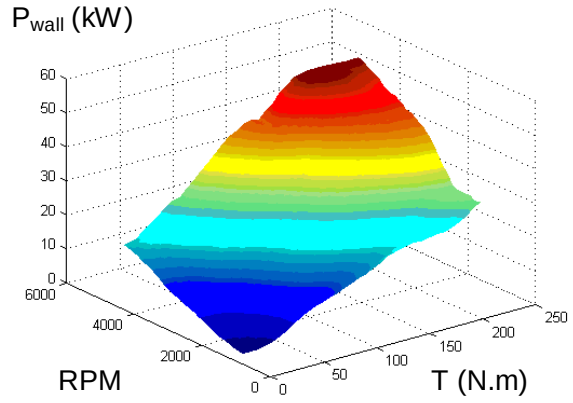


Figure 2 - Cartography of thermal losses towards the coolant circuit [5].

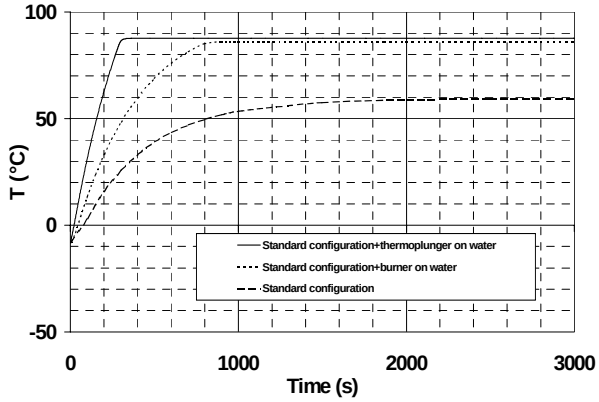


Figure 3 - Predicted impact of additional heating systems [4].

Cartographies are unfortunately unable to take into account variations of other mean parameters (injection timing and profile, mean wall temperature…) without a fastidious battery of simulations.

The objective of this study is to enhance the global simulation tool previously presented [4,5,6]. A "2-zone" combustion model is developed for a greater precision and pollutant formation aspects. Simplified architecture is obtained thanks to a new correlation linking engine settings or parameters, and thermal power lost in the coolant circuit. The final simulation tool architecture is presented in Fig. 4.

The first part of this paper describes the combustion model hypothesis and structure. A description of experimental set-up used to validate the model is then demonstrated. The final part proposes the development of correlations and perspectives.

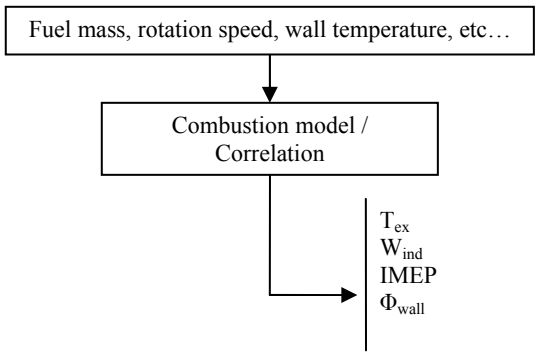


Figure 4 - Final model architecture.

# Two-zone model description

### General outlines

Two-zone models describe more precisely the combustion process than single ones because chemical reactions are taken into account. The unburned zone is crossed by the flame front where products are formed. They are included in the burned zone, whose temperature $T_b$ is assumed to be homogeneous (Fig. 5). The pressure is assumed to be uniform in the whole chamber.

During admission, compression and exhaust phases, the gas is homogeneous. Its composition is assumed to be constant after combustion (the effect of temperature on molar fractions are not taken into account).

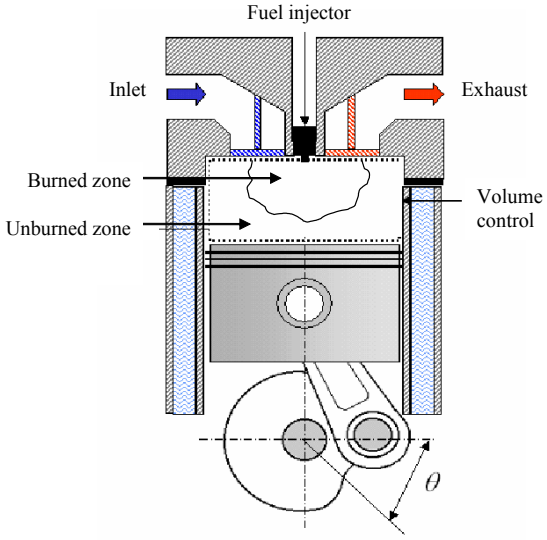


Figure 5 - Two-zone combustion sketch

Mass losses such as blow-by are thus not taken into account in order to simplify equations and reduce computing time. Future studies will be more descriptive on this point.

### Equations

The energy conservation applied to each zone gives the differential equations of burned and unburned zones temperature.

$$\frac{dT_u}{d\theta} = \frac{\left(-P\frac{dV_u}{d\theta} - \frac{dQ_{p,u}}{d\theta} - u_u\frac{dm_u}{d\theta} - h_u.m_{cyl}\frac{dx_b}{d\theta}\right)}{m_u.c_{v,u}} \quad (1)$$

$$\frac{dT_b}{d\theta} = \frac{\left(-P\frac{dV_b}{d\theta} - \frac{dQ_{p,b}}{d\theta} - u_b\frac{dm_b}{d\theta} + h_b.m_{cyl}\frac{dx_b}{d\theta}\right)}{m_b.c_{v,b}} \quad (2)$$

The ideal gas law gives the expression of the cylinder pressure.

$$P = \frac{m_u.R_u.T_u + m_b.R_b.T_b}{V_{cyl}} \quad (3)$$

The mass and volume conservation give relations about $V_u$, $V_b$, $m_u$ and $m_b$.

$$V_u + V_b = V_{cyl} \quad (4)$$

$$m_u + m_b = m_{cyl} \quad (5)$$

The burned fraction $x_b$ follows the largely used predictive Wiebe's relation, [8]:

$$x_b = 1 - \exp\left(-a_w.\left(\frac{\theta-\theta_0}{\Delta\theta}\right)^{M_w+1}\right) \quad (6)$$

Parameters of this relation are $a_w$ (fixed at 6,908 for a final burned fraction of 0,999), the crank angle for start of combustion $\theta_0$ and combustion duration $\Delta\theta$. The form factor $M_w$ describes the energy distribution during combustion processes that is Gaussian if equal to unity. In the present case $M_w = 0.9$.

### Ignition Delay

Ignition delay is defined as the time between start of injection and start of combustion. Many correlations are proposed in literature. They are validated on different kinds of engines and running conditions. Assanis and al. [9] developed a correlation based on steady-state and transient operations for direct injection diesel engines, that suits to the present study. $\tau_{ID}$ depends on the equivalence ratio, the mean temperature *T (K)* and

the pressure *P (bar)* over the ignition interval according to the following equation:

$$\tau_{ID} = 2{,}4.10^{-3} .\phi^{-0,2} .\overline{P}^{-1,02} .\exp\left(\frac{E_a}{R_u.\overline{T}}\right) \qquad (7)$$

$E_a/R_u$ is held constant at a value given by Watson (1980) and used by Assanis. Finally combustion starts when condition (8) is reached.

$$\int_{t_{inj}}^{t_{inj}+\tau_{ID}} \frac{dt}{\tau_{ID}(t)} \approx 1 \qquad (8)$$

**Wall temperature**

The wall temperature is naturally non uniform in the whole chamber. However, Pirotais showed that a unique temperature based on a balance carried out on the 3 main areas of the chamber is acceptable [6]. The spatial average considers the piston, the cylinder liner and the cylinder head (with valves). The average time is obtained with integration of the temperature on the entire cycle. The simulation tool then reconsiders this mean wall temperature after each cycle for heat losses calculation (Fig. 6).

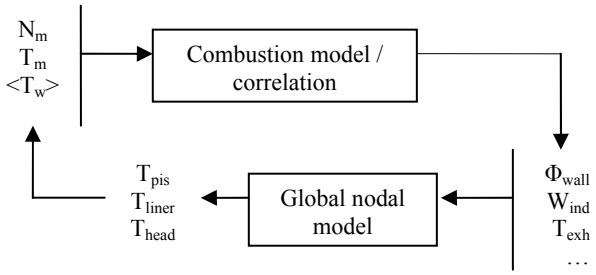


Figure 6 - Computation of mean wall temperature

**Heat transfer**

The expressions of the wall heat transfer and the convective coefficient are presented in Eq. 9 and 10. The heat transfer between the cylinder trapped mass and the surrounding walls is calculated using the Hohenberg relation [10] (Eq. 10).

$$\frac{dQ_p}{dt} = h_g .S_p .(T_g - <\overline{T}_w>) \qquad (9)$$

$$h_g = 130.(10^{-5}.P)^{0,8}.(u_{pis}+1{,}4)^{0,8}.T_g^{-0,4}.V^{-0,06} \qquad (10)$$

This correlation is relatively well adapted to direct injection diesel engines since high pressure injection systems allow reduction in soot particles formation. Thus the radiative part of heat transfer is not taken into account in Eq. 10. However, the convective heat transfer will be accurately determined within future studies on current automotive engines. Wall areas of burned and unburned zones are calculated thanks to the burned fraction correlation presented in Eq. 6, [11].

$$S_{p,u} = \left(\frac{\pi.d_s^{\,2}}{2} + \frac{4.V_{cyl}}{d_s}\right).\left(1-\sqrt{x_b}\right) \qquad (11)$$

$$S_{p,b} = \left(\frac{\pi.d_s^{\,2}}{2} + \frac{4.V_{cyl}}{d_s}\right).\sqrt{x_b} \qquad (12)$$

**Chemistry of combustion**

The combustion reaction was written for a $C_{10,8}H_{18,7}$ fuel with properties found in [12]. The combustion equation is:

$$\begin{aligned}\phi\varepsilon.C_{10,8}H_{18,7} + (0{,}21.O_2 + 0{,}79.N_2) \rightarrow \nu_1.CO_2 + \\ \nu_2.H_2O + \nu_3.N_2 + \nu_4.O_2 + \nu_5.CO + \\ \nu_6.H_2 + \nu_7.H + \nu_8.O + \nu_9.OH + \\ \nu_{10}.NO\end{aligned} \qquad (13)$$

where Φ is the equivalence ratio. $CO_2$, $H_2O$, $N_2$ and $O_2$ come from the complete combustion, CO, $H_2$, H, O, OH, and NO from dissociation and recombination reactions. $\upsilon_i$ represents the mole fraction of the constituent i, and ε is the fuel quantity for one mole of products at stoechiometry. Species conservation relations combined with equilibrium constants expressions give a non linear system solvable with different methods. Olikara and Borman [13] described a complete method using a Newton–Raphson algorithm. This method is also used in this study. Specific heat and molar enthalpies expressions are temperature dependent according to relations of Kee and al. [14].

**Modelling of nitric oxides formation**

In the present study the nitric oxide formation is assumed to follow the largely used extended Zeldovitch mechanism [15]. The following three equations are considered (Eq. 14).

$$N_2 + O \leftrightarrow N + NO$$

$$k_{1,f} = 7{,}6\times10^7.\exp\left(-\frac{38000}{T}\right) \qquad (14.a)$$

$$NO + O \leftrightarrow N + O_2$$

$$k_{2,f} = 1{,}5\times10^3.T.\exp\left(-\frac{19500}{T}\right) \qquad (14.b)$$

$$NO + H \leftrightarrow N + OH$$

$$k_{3,f} = 2 \times 10^{8}.\exp\left(-\frac{23650}{T}\right) \qquad (14.c)$$

$k_i$ represents the reaction rate constants. Correlations were taken according to Heywood studies [16].

According to chemical dissociations and assuming that [N] concentration remains constant, the evolution of [NO] concentration is expressed in Eq. 15.

$$\frac{1}{V}\frac{d([NO]V)}{dt} = \frac{2(1-\beta^2)R_1}{\left(1+\beta\frac{R_1}{R_2+R_3}\right)} \qquad (15)$$

where

$$R_1 = k_{1,f}\,[N_2]_e.[O]_e$$
$$R_2 = k_{2,f}\,[NO]_e.[O]_e$$
$$R_3 = k_{3,f}\,[NO]_e.[H]_e$$
$$\beta = [NO]/[NO]_e$$

and index *e* denotes equilibrium.

**Time step**

A 0,1 crank angle resolution gives a good compromise between computing time and accuracy.

## Comparison of calculated and measured data

**Test bench**

Any prediction model has to be validated thanks to diagrams measured on the test bench. Experimental results on a naturally aspired single-cylinder direct injection diesel engine are available, [17]. The main design parameters are presented in Tab. 1. The complete description of tests can be found in [17].

| | |
|---|---|
| **Constructor** | Listter – Petter |
| **Bore** | 95,2 mm |
| **Stroke** | 88,94 mm |
| **Displacement** | 633 $cm^3$ |
| **Compression ratio** | 19.22 : 1 |
| **Cooling system** | Forced air circulation |

Table 1 – Engine technical features

**Comparison**

These measurements are compared to the results of the previously described model. An example of pressure diagrams comparison is plotted in Fig. 7.

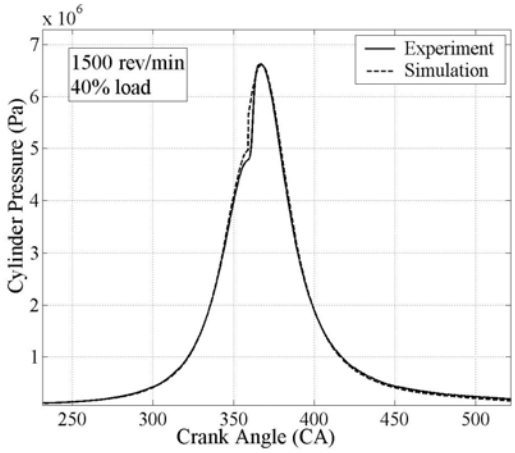


Fig. 7 – Comparison between the experimental and numerical pressure diagrams

Computer modelling gives good agreements with experiments for pressure diagrams and efficiency coefficients. The indicated efficiency $\eta_i$, Indicated Mean Effective Pressure *IMEP* and volumetric efficiency $\eta_v$ comparison are shown in Tab. 2.

| | Model | Experiment |
|---|---|---|
| $\eta_i$ *(%)* | 50,2 | 49,7 |
| *IMEP (bar)* | 4,9 | 5 |
| $\eta_v$ *(%)* | 85,2 | 85,7 |

Table 2 – Engine performances comparison (1500 rev/min, 40% load)

In the whole range of tests, the low average error between numerical results and measured values proves reliability of the model.

## Simulation results and correlations

**Objectives**

As already mentioned, the previous simulation program of Pirotais [6] needs a complete cartography of thermal losses towards the coolant loop. The aim of this study is to remove this step by using a correlation for indicated performance, deduced from two-zone modelling results.

**Theoretical analysis**

*IMEP* can be expressed from volumetric efficiency, equivalence ratio and indicated efficiency definitions (Eq. 18-22).

$$IMEP = \eta_i . \eta_v . \phi . \frac{LHV}{\sigma} . \frac{P_{atm}}{R_{atm} . T_{atm}} \quad (18)$$

with

$$\eta_v = \frac{m_{air,aspired}}{m_{air,atmospheric\ conditions}} \quad (19)$$

$$\phi = \frac{m_{diesel,injected}}{m_{air,aspired}} . \sigma \quad (20)$$

$$IMEP = \frac{W_{ind}}{V_c} \quad (21)$$

$$\eta_i = \frac{W_{ind}}{m_{diesel,injected} . LHV} \quad (22)$$

**Speed and load variations**

The experimental design method was applied to determine which parameters have a significant effect on indicated efficiency. The results revealed that speed, load and injection timing have major influence. The effect of rotation speed and load are studied first. The results are presented in Fig. 8.

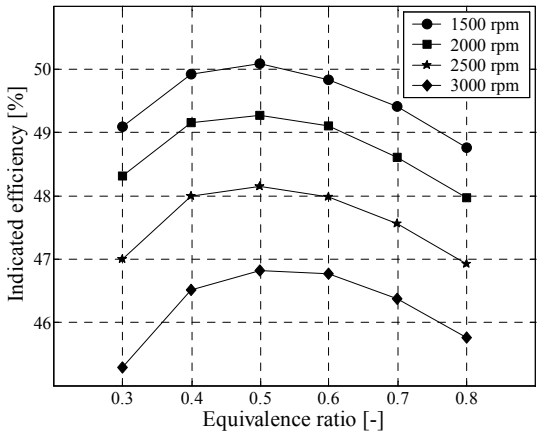


Fig. 8 – Evolution of efficiency with different engine speeds and loads

When the equivalence ratio is under 0.5-0.6, efficiency increases with a negative exponential trend. It decreases for higher values. Considering transient conditions and low loads during cold start driving tests, this study focuses on the first part of the curves.

The relation deduced from results for equivalence ratio under 0.5 is given in Eq. 23.

$$\eta_i = \eta_0 - \alpha . \exp\left(-\frac{\phi}{\phi_0}\right) \quad (\phi < 0.5) \quad (23)$$

Each parameter follows a linear dependence with engine speed (Eq. 24).

$$p_i = A_i + B_i . N \quad (24)$$

where $p_i$ represents $\eta_0$, $\alpha$ or $\Phi_0$. $A_i$ and $B_i$ are linear results from fitting database (Tab. 3).

| Parameter | $A_i$ | $B_i$ |
|---|---|---|
| $\eta_0$ | 53,3 | $-2,1.10^{-3}$ |
| $\alpha$ | 34,6 | $5,3.10^{-3}$ |
| $\Phi_0$ | $5,9.10^{-2}$ | $1.10^{-5}$ |

Table 3 – Linear coefficients for Eq. 24

Considering the whole range of load and rotation speed, the maximum error between simulated and correlated indicated efficiencies remains under 10% (Fig. 9).

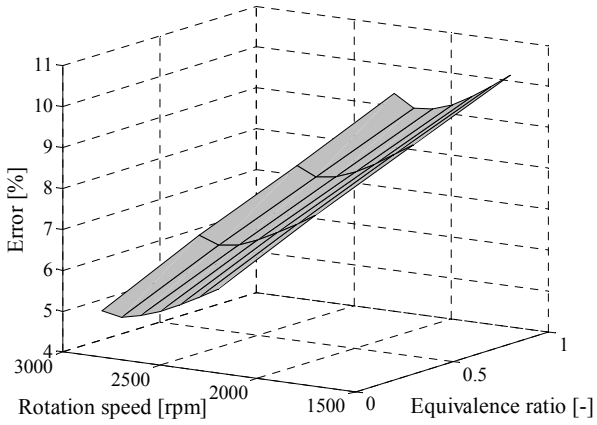


Fig. 9 – Error between simulated and correlated indicated efficiencies

This correlation only takes into account speed and load variations. For combustion engine behaviour, it should be completed by adding other physical parameters. Nevertheless the accuracy of the present correlation proves that this predictive method can be explored.

**Injection timing variations**

Injection timing and combustion duration are physically linked [16]. However the experimental design method shows that combustion duration has a minor effect on indicated performance compared to injection timing. A sensitivity study on injection timing is then shown.

Fig. 10 presents the evolution of pressure curves with injection timings between 5 and 25 degrees BTDC. As is well known, peak pressure increases with injection timing [7].

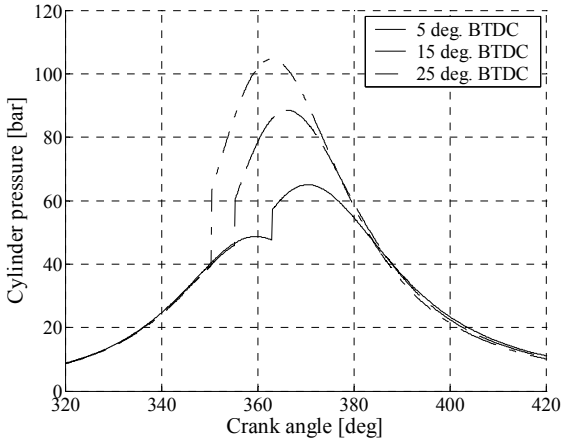


Fig. 10 – Pressure diagrams for different injection timings

Fig. 11 shows the evolution of efficiency with the injection timing in a larger range. Maximum value appears around 15 deg. BTDC. These results show that injection timing must appear in global indicated efficiency correlation. Studies are currently carried out to define how this parameter must be taken into account in the reduced model.

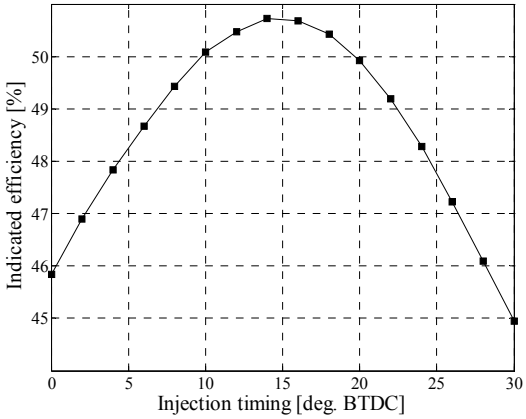


Fig. 11 – Indicated efficiency evolution with injection timing (1500 rpm – 50% load).

**Nitric oxide formation**

As already shown, the main purpose of this paper is to predict engine performance. Last objectives of this study are AHS development and characterization of their effects on the warm up phase, including emissions. Simulations of NO formation are thus computed. An example is given in Fig. 12. The diagram trend agrees with Rakopoulos results [19] and validates the model. After reduction of the combustion model and its introduction in the global simulation tool, the comparison of the effects on emissions can become decisive for the AHS future classification.

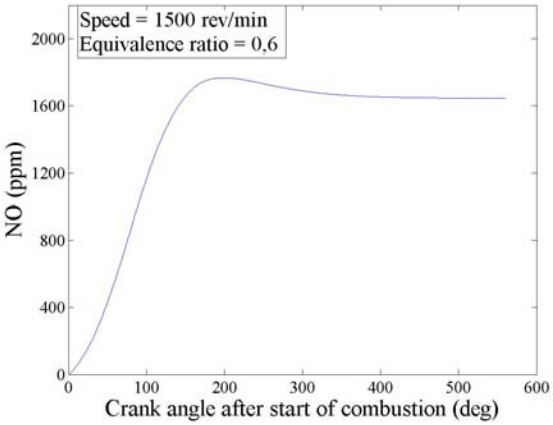


Fig. 12 – Nitric oxide formation (N = 1500 rev/min, φ = 0.5)

## Conclusions and perspectives

A correlation for the prediction of indicated efficiency has been demonstrated. This correlation was based on numerical results from a two-zone combustion model detailed in this paper. For the direct injection diesel engine addressed in this paper, simulations proved that performance and engine settings can be correlated. Future studies aim to validate the present method in a larger range of engine types and specially car engines (turbo-charged, direct injection, etc…). Correlations must also include other parameters such as injection timing.

Further studies on the convective transfer coefficient must also be realised. Technical literature proves how difficult it is to well express the wall heat transfer. The most accurate correlation must be adapted and validated on turbocharged direct injection diesel engines. Exhaust Gas Recirculation (EGR) will be taken into account. Its effects on NO, soot emissions and on engine efficiency must appear in the final conclusions of the study. A single fuel injection type was computed here considering the experimental engine equipment. According to real trends several injections can be used for pollutant formation reduction.

## References


[1] Haubner FG, Klopfstein S, Koch F. *Cabin heating – a challenge for the TDI cooling system*. Conference SIA 2000/03/23, Lyon, may 2000.

[2] Eilemann A, Kampf H. *Comfort-Management*. SAE Paper N° 2001-02-1738, 2001.

[3] De Pelsemaeker G, Karl S. *Thermal deficit and additional heating systems: actual and future trends.* Conference SIA 2000/03/24, Lyon, may 2000.

[4] Pirotais F, Bellettre J, Le Corre O, Tazerout M, De Pelsemaeker G and Guyonvarch G. *A model of energetic interactions between a car engine, the cabin heating system and the electrical system*. SAE Paper N° 2002-01-2224, 2002.

[5] Pirotais F, Bellettre J, Le Corre O, Tazerout M, De Pelsemaeker G and Guyonvarch G. *A diesel engine thermal transient simulation. Coupling between a combustion model and a thermal model*. SAE Paper N° 2003-01-0224, 2003.

[6] Pirotais F. *Contribution à la modélisation du flux thermique disponible pour le chauffage d'un habitacle d'automobile après un démarrage à froid.* Université de Nantes, PhD Thesis (in french), 2004.

[7] Kouremenos DA, Houtalas DT, Binder KB, Raab A, Schnabel MH. *Using Advanced Injection Timing and EGR to improve DI Diesel Engine Efficiency at Acceptable NO and Soot Levels.* SAE Paper N° 2001-01-0199, 2001.

[8] Rousseau S. *Contribution à l'étude du cycle thermodynamique de moteurs de cogénération fonctionnant au gaz naturel en mélange pauvre.* Université de Nantes, PhD Thesis (in french), 1999.

[9] Assanis DN, Filipi ZS, Fiveland SB, Syrimis M. *A predictive ignition delay correlation under steady-state and transient operation of a direct injection diesel engine.* Paper n°00-ICE-231, ICE-Vol. 33-2, 1999 Fall Technical Conference ASME, 1999.

[10] Hohenberg GF. *Advanced approaches for heat transfer calculations.* SAE Paper N° 790825, 1979.

[11] Tazerout ML. *Etude des possibilités d'amélioration du rendement à charge partielle des moteurs à allumage commandé.* Université Catholique de Louvain, PhD Thesis (in french), 1991.

[12] Turns SR. *An introduction to combustion. Concepts and applications.*McGraw-Hill International Editions, 1996.

[13] Olikara C, Borman GL. *A computer program for calculating properties of equilibrium combustion products with some applications to I.C. engines.* SAE Paper N° 750468, 1975.

[14] Kee RJ, Rupley FM, Miller JA. *The chemkin thermodynamic data base.* Sandia Report, SAND87-8215B – UC-4, 1992.

[15] Lavoie GA, Heywood JB, Keck JC. *Experimental and theoretical study of nitric oxide formation in internal combustion engines.* Combustion science and technology, 1:313-326, 1970.

[16] Heywood JB. *Internal Combustion Engine Fundamentals.* Number ISBN 0-07-100499-8, McGraw-Hill Editions, 1988.

[17] Bilcan A. *Contribution à l'étude du cycle thermodynamique de moteurs fonctionnant en Dual-Fuel.* Université de Nantes, PhD Thesis (in french), 2003.

[18] Monaghan ML. *Engine Friction – A change in emphasis.* The Instm. Mech. Eng. Tribology lecture, 1987.

[19] Rakopoulos CD, Rakopoulos DC, Giakoumis EG, Kyritsis DC. *Validation and sensitivity analysis of a two-zone diesel engine model for combustion and emissions prediction*. Energy Conversion and Management 45 (2004) 1471-1495, 2004.